Large-Scale Synthesis of Flexible Free-Standing SERS Substrates with High Sensitivity: Electrospun PVA Nanofibers Embedded with Controlled Alignment of Silver Nanoparticles

Dian He, Bo Hu, Qiao-Feng Yao, Kan Wang, and Shu-Hong Yu*

Division of Nanomaterials & Chemistry, Hefei National Laboratory for Physical Sciences at Microscale, The School of Chemistry & Materials, University of Science and Technology of China, Hefei 230026, People's Republic of China

ABSTRACT A new and facile way to synthesize a free-standing and flexible surface-enhanced Raman scattering (SERS) substrate has been successfully developed, where high SERS-active Ag dimers or aligned aggregates are assembled within poly(vinyl alcohol) (PVA) nanofibers with chain-like arrays *via* electrospinning technique. The aggregation state of the obtained Ag nanoparticle dimers or larger, which are formed in a concentrated PVA solution, makes a significant contribution to the high sensitivity of SERS to 4-mercaptobenzoic acid (4-MBA) molecules with an enhancement factor (EF) of 10^9. The superiority of enhancement ability of this Ag/PVA nanofiber mat is also shown in the comparison to other substrates. Furthermore, the Ag/PVA nanofiber mat would keep a good reproducibility under a low concentration of 4-MBA molecule (10^{-6} M) detection with the average RSD values of the major Raman peak less than 0.07. The temporal stability of the substrate has also been demonstrated. This disposable, easy handled, flexible free-standing substrate integrated the advantages including the superiority of high sensitivity, reproducibility, stability, large-scale, and low-cost production compared with other conventional SERS substrates, implying that it is a perfect choice for practical SERS detection application.

KEYWORDS: Ag dimer · chain-like arrays · SERS · electrospinning · free-standing · large scale

Since surface-enhanced Raman scattering (SERS) was discovered 30 years ago,[1−3] it has inspired a worldwide effort to explore its mechanism both theoretically and experimentally. SERS offers a tremendous enhancement of the intensity of the vibrational signals over 10 orders of magnitude, which has opened a new avenue for conventional Raman spectroscopy and made it an ultrasensitive analytical tool down to single-molecule detection,[4] ranging from life science[5−7] to environmental science.[8,9] It is widely accepted that electromagnetic enhancement and chemical enhancement are responsible for SERS enhancement.[10,11] The former makes the major contribution that is associated with the localized surface plasmon resonances occurring at the surfaces of roughened metal substrates or metal clusters, and the latter is several orders of magnitude smaller than the former, which is associated with the direct charge transfer or indirect electron−hole pair excitation processes.

Progress has been made in controlling the assembly of silver or gold nanoparticles into specific structures that would be employed as SERS substrates.[12,13] Electron beam lithography,[14] nanosphere lithography,[15] focused ion beam pattering,[16] and vacuum evaporation[17] are currently available techniques for fabrication of well-ordered, periodic silver or gold nanoparticle arrays with desired geometries. The substrates obtained by these techniques show a large Raman enhancement ability and a good SERS reproducibility. Nevertheless, they are high cost-demanding and hard to extend to large scales for routine SERS detection. On the other hand, novel strategies have been devoted to developing stable, inexpensive, large-scale, and reliable SERS substrates, such as Ag-coated silicon nanowire arrays,[18,19] Ag NP-impregnated polycarbonate,[20] and Au NP-decorated porous aluminum membranes.[21] However, the sensitivity of these SERS substrates remains modest owing to a limited number of the so-called hot spots. Designing and assembling highly effective substrates for SERS application still requires further improvement.

The first single-molecular surface-enhanced Raman scattering (SM-SERS) studies were performed on aggregates

*Address correspondence to shyu@ustc.edu.cn.

Received for review July 16, 2009 and accepted November 17, 2009.

Published online November 23, 2009. 10.1021/nn900812f

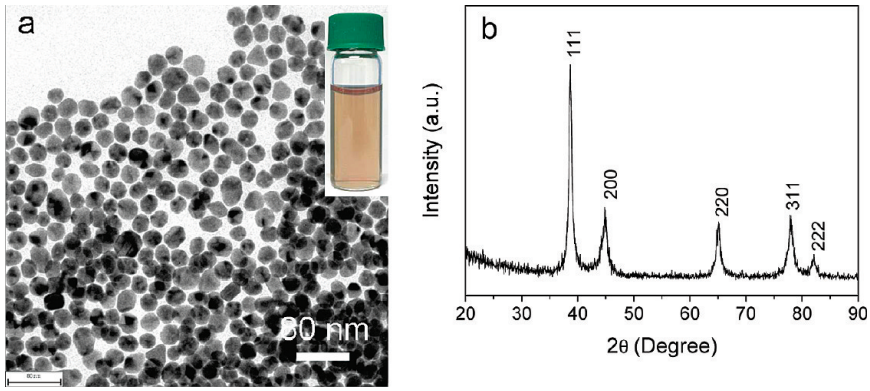

Figure 1. (a) Typical TEM image of Ag NPs in aqueous system using L-lysine as reducing agent and soluble starch as capping agent *via* microwave irradiation at 150 °C for 10 s; the inserted image is the photograph of the aqueous dispersions of the Ag NPs. (b) Typical XRD pattern of the obtained Ag NPs.

of silver colloidal nanoparticles.[4,22−24] Subsequently, more experiments gave evidence that the extremely high SERS enhancement factors and single-molecule sensitivity came from the compact, nonfractal silver or gold particle cluster, dimer or larger for the reason that the electromagnetic field in the gap region of them can be drastically amplified.[25−27] It is also demonstrated that the enhancement factors of multiparticle aggregates for both silver and gold would be several orders of magnitude higher than isolated nanoparticles, especially for the nonresonant molecules.[25] Therefore, the aggregates of silver or gold nanoparticles are the best suitable structures for optimal SERS substrates.[25,28−30]

In this paper, we present a new class of highly sensitive, reproducible, stable, portable, large-scale, and inexpensive SERS substrates fabricated by electrospinning technique where the SM-SERS-active silver dimers or larger were assembled in PVA nanofibers as prospected. At the beginning, nearly monodisperse Ag NPs were synthesized in large quantities *via* a microwave-assisted method. Then poly(vinyl alcohol) (PVA), a nontoxic, biocompatible polymer, a popular material used in electrospinning, was employed, not only as the host matrix but also as an organic additive inducing the aggregation of individual Ag NPs. Subsequently, the resulting SM-SERS-active aggregates were assembled in PVA nanofibers by electrospinning process, and at the same time, the aggregation of Ag NPs "froze up". The coating polymer can provide protection for the active Ag aggregates from the surrounding environment. Under a moderate solvent, the coating polymer would slightly swell and the small target molecules would permeate into the polymer and access the hot spots easily. Thus, the obtained substrates possess an extremely long lifetime and high sensitivity. On the other hand, the obtained substrate is completely free-standing and can be tailored freely due to the flexibility of polymer. What is more, both the fabrication of high sensitivity Ag aggregates and the electrospinning process are low-cost and high-throughput. These disposable SERS substrates would bring great convenience to the routine SERS detection and avoid cross contamination. All of these excellent properties mentioned above made the obtained substrate a really perfect choice for routine SERS detection application.

RESULTS AND DISCUSSION

Monodipersed Silver Nanoparticles. A representative transmission electron microscope (TEM) image of Ag NPs synthesized by microwave irradiation is shown in Figure 1a, which confirmed the generation of highly crystalline nanoparticles with a nearly spherical shape. A histogram of the particle size distribution indicated the mean particle diameter of 26 nm (see Supporting Information Figure S1). The X-ray diffraction (XRD) pattern of the nanoparticles (Figure 1b) showed a face-centered cubic (fcc) silver crystal structure (JCPDS card No. 04-0783). The resulting particles, which were readily redispersed in water, presented a transparent light-brown suspension of well-dispersed Ag NPs (Figure 1a). The aqueous solution was stable without precipitation for months at room temperature.

Silver Dimers and Silver Aggregates. The as-prepared silver colloids were washed with deionized water and centrifuged three times. Then they were redissolved in 7 wt % PVA aqueous solution. Due to the high hydrophilic property, Ag NPs were miscible with hydrophilic PVA solution. After incubated in a shaker at 40 °C for 5 h, the mixture solution presented a color change from light-brown to green, which indicated the aggregation of Ag NPs. Previous studies on the interaction between PVA and metal were focused on synergistic soft−hard template effect of guiding the oriented growth.[31−33] In this work, we find that PVA can also induce the self-assembling of Ag NPs to Ag dimers or larger or nanochains in a concentrated aqueous PVA solution.

To further understand the process of formation of Ag aggregates, we have investigated the interaction between Ag NPs and PVA. The stabilizer starch adsorbed on the surface of spherical Ag NPs has been partially removed by the process of washing with deionized water and being centrifuged three times. After incubating in a shaker at 40 °C for 5 h, the surface of Ag NPs was partially capped with the new additive PVA. The difference of capping additive between the monodispersed Ag NPs and aggregates was shown in FTIR spectra (see Supporting Information Figure S2). A wide, strong peak at 3425 cm^{-1} was shown due to the stretching vibration of −OH in the PVA chains, which meant that the Ag aggregates were coated with PVA. Magnified TEM image revealed that adjacent Ag NPs were often in close contact among the aggregates and were cov-

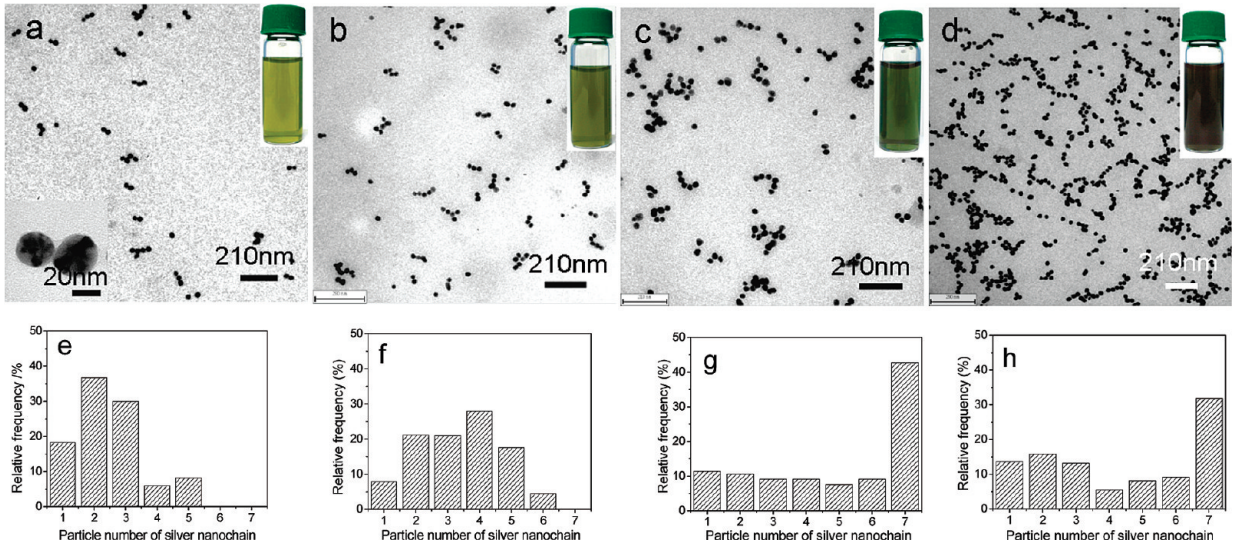

Figure 2. Typical SEM image of Ag NP aggregates in PVA aqueous solution with a PVA/Ag molar ratio of (a) 530:1, (b) 530:2, (c) 530:3, and (d) 530:4. Inset shows the photographs of the samples. (e−h) Corresponding distribution frequency of nanoparticle numbers appearing in silver NP aggregates. For example, the number 7 represents that the particle number in each aggregate is 7 or more than 7.

ered by a uniform 1 nm thick layer of organic materials, which appeared to bridge neighboring Ag NPs (inset in Figure 2a). There were still some Ag NPs uncoupled in the Ag/PVA composite solution.

Under the circumstances of restricted reaction time and the same concentration of PVA aqueous solution, the extent of aggregation and the sizes of the nanoclusters were strongly dependent on the amount of Ag NPs added.[34] When a smaller amount of Ag NPs was added in 7 wt % PVA aqueous solution, with a PVA/Ag molar ratio (PVA in terms of repeat units and Ag in terms of atoms) of 530:1, and incubated in a shaker at 40 °C for 5 h, the composite solution appeared the color of pale green. TEM image (Figure 2a) showed clearly the aggregation of Ag NPs and the formation of Ag dimers or trimer. When the amount of Ag NPs was added with a PVA/Ag molar ratio of 530:2, the TEM image (Figure 2b) showed clearly the formation of Ag tetramer or larger also with some dimer and trimer. The aggregated sample consisted mainly of discrete short nanochains with lengths of 90−120 nm (Figure 2b), equivalent to 3−4 isomeric 26 nm Ag nanoparticles. The Ag/PVA solution appeared a color of green. When the amount of Ag NPs was added with a PVA/Ag molar ratio of 530:3, the TEM image (Figure 2c) clearly showed the formation of Ag nanoclusters. The aggregated sample mainly consisted of bifurcated and looped nanochains with 7−10 isomeric 26 nm Ag nanoparticles. The composite solution appeared dark green. When a larger amount of Ag NPs with a PVA/Ag molar ratio of 530:4 was added, random aggregates were obtained and the solution appears greenish black (Figure 2d).

The combination of Ag NPs and PVA is stable enough that the short chain-like structures would not be disrupted from heating dispersions at 70 °C for 1 h or sonication at room temperature for 30 min.

Optical Properties of Silver Nanoparticles. It is well-known that the optical properties of Ag NPs are strongly dependent on their sizes and shape. The UV/vis spectra (Figure 3a) of monodispersed Ag NPs synthesized by microwave displayed a strong extinction band with a maximum at 403 nm, which was a characteristic plasmon resonance band of isolated spherical silver nanoparticles.[44] When the PVA solution was introduced, the Ag colloids exhibited two absorbance bands. One was near 403 nm, indicating the uncoupled Ag NPs existed in the composite solution, and the other absorbance band red-shifted with the increase of Ag/PVA molar ratio. The appearance of this long-wavelength plasmon band is a clear indication of the formation of aggregated nanostructures. Once the nanoparticles form aggregates, their plasmon modes interact with each other and form a new plasmon band, which is associated with the surface plasmon coupling between adjacent Ag NPs.[35,36] In addition, the new band became further broadened and red-shifted with the increase of the molar ratio of Ag/PVA in the Ag/PVA solution, indicating a stronger aggregation state and a larger distribution in the sizes of the aggregated nanoparticles.

Silver Dimers and Nanochains Assembled within PVA Nanofibers. Electrospinning technology is a versatile and effective method to generate fibers with a diameter of several tens to hundreds of nanometers from a variety of materials.[37,38] The Ag/PVA nanofiber nonwoven mat over 80 cm^2 can be produced by electrospinning a 0.3 mL Ag/PVA solution (with PVA/Ag molar ratio of 530:3) for 1 h by electrospinning (Figure 4a), indicating that it was a really facile method with high output. The Ag/PVA nanofiber mat, appearing the color of green, was not as deep as the corresponding electrospinning solu-

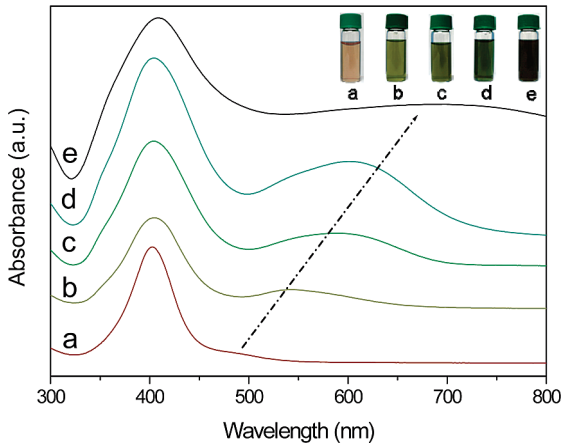

Figure 3. UV/vis absorption spectra of Ag nanoparticles upon addition of different amounts of Ag with PVA/Ag of (a) 0:1, (b) 530:1, (c) 530:2, (d) 530:3, and (e) 530:4. Inset is the photograph of the corresponding Ag/PVA solution.

tion. The aqueous PVA solution was transparent, so the Ag/PVA blend solution appeared the color of Ag aggregates. In addition, the solid PVA nanofiber mat without addition of Ag nanoparticles appeared a color of white, thus the Ag/PVA nanofiber mat appeared the color of integrated PVA and Ag aggregates, which would be a lighter color than Ag aggregates in PVA solution.

Typical SEM image of Ag/PVA nanofibers produced by electrospinning is shown in Figure 4b, which shows a three-dimensional network structure consisting of a large quantity of randomly deposited fibers, and the individual fiber has a high aspect ratio and a smooth surface. The average diameter and length of Ag/PVA nanofibers were about 170 nm and several millimeters, respectively. TEM images in Figure 5 clearly showed that Ag aggregates were embedded in PVA matrix and assembled to some ordered linear chain-like structures along the fiber axial direction. Contrast to the solution before electrospinning with a random dispersion of the aggregates, we can conclude that the Ag NP aggregates with chain-like arrays in the PVA matrix resulted from the electrospinning process.

When a high voltage was applied to the blend solution, the whole solution was polarized and the PVA-capped Ag aggregates became positively charged on one side and negatively charged on the other. Due to the static absorption among the polarized Ag aggregates, they tended to form a self-assembling linear chain-like structure oriented along the electric field in the blend solution.[39,40] When the repulsive force within the charged solution was larger than its surface tension, a jet would erupt from the tip of the spinneret. Although the jet was stable near the tip of the spinneret, it soon entered a bending instability stage, and the formation of nanofibers was mainly achieved by the stretching and acceleration of the fluid filament in the instability region as the solvent evaporated. During the formation of nanofibers, Ag aggregates were totally embedded in PVA nanofibers simultaneously, in order to reduce the specific surface area and the surface Gibbs free energy of individual nanofiber. This result can be confirmed by both SEM and XPS. Seen from the magnified SEM image in the inset of Figure 4b, the surface of each nanofiber was smooth and there were no particles raised on the surface of fibers. Also, there were no obvious peaks of silver element observed by XPS (see Supporting Information Figure S3). The schematic diagram of the Ag/PVA nanofiber formation is illustrated in Figure 6.

By electrospinning an aqueous Ag/PVA blend solution, PVA was split into long continuous fibers, but the low concentration of Ag aggregates in the blend solution (with Ag/PVA molar ratio less than 4:530) together with the bending instability of electrospinning process could result in the discontinuousness of Ag NP aggregates dispersed in the PVA nanofibers. The Ag aggregates, if once trapped in fibers, tended to pack a linear chain-like structure along the axial direction of fibers, seldom with total separation in the fibers. The presence of Ag elements in the nanofibers was demonstrated by the energy-dispersive spectrum (EDS) shown in Figure 7.

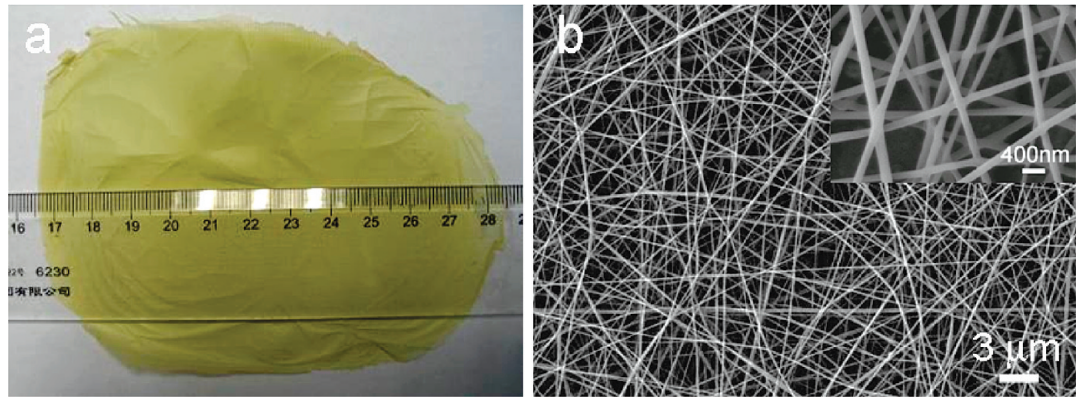

Figure 4. (a) Photograph of Ag/PVA nanofiber mat (with a PVA/Ag molar ratio of 530:3) by electronspinning for 1 h. (b) Typical SEM image of Ag/PVA nanofiber mat. Inset shows the high magnified SEM image.

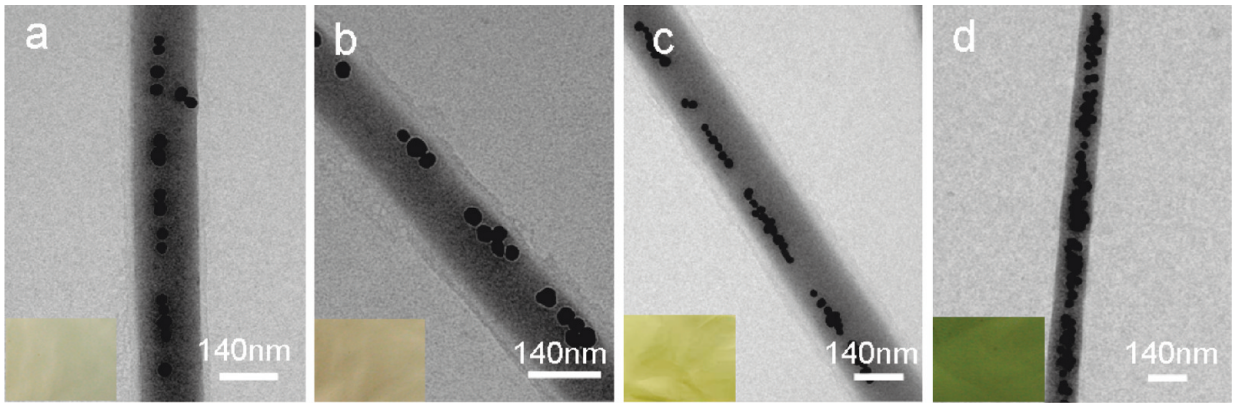

Figure 5. Typical TEM image of Ag/PVA nanofibers with the molar ratio of PVA/Ag (a) 530:1, (b) 530:2, (c) 530:3, and (d) 530:4. Inset is the photograph of the corresponding Ag/PVA nanofiber mat.

Electrospinning the Ag/PVA solution with different molar ratio of PVA/Ag resulted in a series of various Ag NP aggregates assembled within PVA nanofibers. The extent of aggregation and sizes of the aggregates assembled in nanofibers were strongly dependent on the aggregates existing in corresponding electrospinning solution, which was dependent on the amount of Ag NPs added in pure PVA solution. The Ag NPs would tend to aggregate further with the reaction time increased and the electrospinning process can "freeze up" the aggregation state of Ag NPs and prevent them from further aggregation. Thus, various arrays of Ag NP aggregates in PVA fibers would be obtained *via* electrospinning technique by adjusting the quantity of Ag NPs which were added in PVA solution.

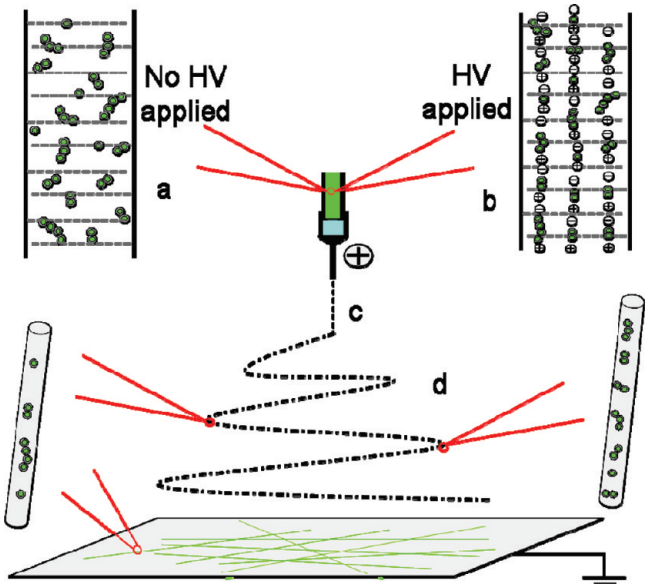

Figure 6. Simplified schematic representation of the formation of chain-like arrays of Ag NP aggregates within PVA nanofibers. (a) Random dispersion of Ag aggregates in PVA solution before a high voltage was applied. (b) When a high voltage was applied to the blend solution, the whole solution was polarized and the PVA-capped Ag NP aggregates became positively charged on one side and negatively charged on the other. They would align themselves by electrostatic attraction in the direction of the electric filed. (c) Stable region near the tip of the spinneret. When the repulsive force within the charged solution was larger than its surface tension, a jet would erupt from the tip of the spinneret. (d) Instability region where most nanofibers were formed by the stretching and acceleration of the fluid filament as the solvent evaporated.

Surface Enhancement Raman Scattering Characterization. The assembled Ag NP aggregates in PVA fibers had high local electromagnetism, and they could be used as SERS substrates for molecular sensing with high sensitivity and specificity. The electrospun Ag/PVA nonwoven mat is easy to tailor into any desired shape for routine SERS analysis (see Supporting Information Figure S4). The SERS measurements used 4-MBA as probing molecules to study the enhancement effects of the Ag/PVA nanofiber mats because 4-MBA has distinct Raman features and it is easy to absorb on the surface of Ag NPs for the bond of −SH. Significantly, PVA is only moderately resistant to ethanol, so that 4-MBA molecules can permeate into the fiber, access the Ag NPs, and be trapped in the hot spot region in an ethanol solution. Additionally, the Ag/PVA nanofiber mat after being immersed in 4-MBA ethanol solution still keeps its net-like structures (see Supporting Information Figure S5). As a result, the trace level of 4-MBA on our Ag/PVA nanofibers is 10^{-9} M (see Supporting Information Figure S6).

Influence of Different Ag NP Aggregates Assembled in PVA Nanofibers. Figure 8 shows a set of SERS spectra of 4-MBA molecules absorbed on different Ag aggregates assembled in PVA nanofiber mats at an excitation wavelength of 514.5 nm. The observed Raman bands that can be assigned to 4-MBA molecules include $\nu(CC)_{ring}$ ring-breathing modes (1036 cm^{-1}), $\nu(CC)_{ring}$ ring stretching (1557 and 1584 cm^{-1}), and $\delta(CH)$ bends (1117 and 1152 cm^{-1}).

In this study, the intensity of the $\nu(CC)_{ring}$ ring-breathing modes (1036 cm^{-1}) was chosen to estimate the enhancement factor (EF) of the Ag/PVA nanofiber mats through the following equation:

$$EF = [I_{SERS}]/[I_{Raman}] \times [N_{bulk}]/[N_{ads}] \quad (1)$$

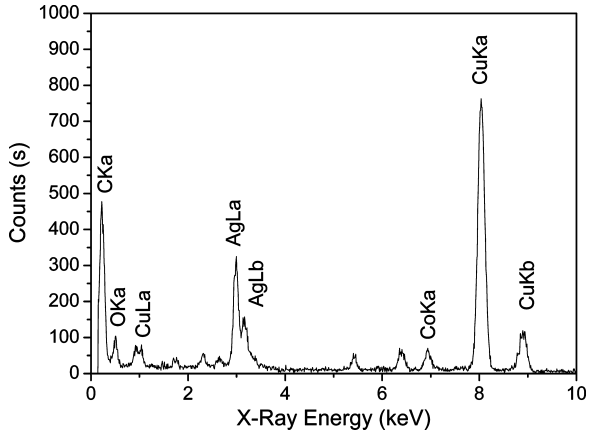

Figure 7. EDS taken on the Ag/PVA nanofiber mat with the molar ratio of PVA/Ag 530:4.

where I_{SERS} is the intensity of a vibrational mode in the surface-enhanced spectrum, I_{Raman} is the intensity of the same mode in the Raman spectrum, N_{bulk} is the number of bulk molecules probed for a bulk sample, and N_{ads} is the number of molecules adsorbed on the SERS-active substrate. Furthermore, the Raman spectrum of aqueous 4-MBA solution (2 mmol/L) was used for the enhancement factor for the "bulk" values (see Supporting Information Figure S7). N_{bulk} and N_{ads} are estimated by approximate calculation by monolayer-absorbed mode (see Supporting Information).[41] The EF values for 4-MBA on different Ag aggregates assembled in PVA nanofiber mats were calculated using eq 1 and are given in Table 1.

The interesting observation was the difference in EF values for each of the Ag/PVA nanofiber mats with different molar ratios of PVA/Ag. As the molar ratio of Ag/PVA in the nanofiber mat increased, both the planar density of Ag NP aggregates on the per unit area of the nanofiber mat and the number of 4-MBA molecules adsorbed on the per unit area of the nanofiber mat increased, but the intensity of the Raman peak and

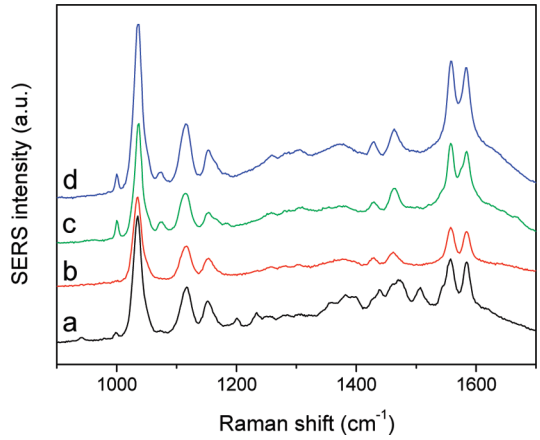

Figure 8. SERS spectra of 2 mM 4-MBA molecules collected on a set of Ag/PVA nanofiber mats with different PVA/Ag molar ratios of (a) 530:1, (b) 530:2, (c) 530:3, and (d) 530:4. The electrospinning time is 1 h, and the acquisition time is 5 s.

TABLE 1. EF of 4-MBA Molecules on a Set of Ag/PVA Nanofiber Mats with Different PVA/Ag Molar Ratio

PVA/Ag molar ratio	EF
530:1	8.8×10^9
530:2	4.7×10^9
530:3	9.0×10^9
530:4	7.7×10^9

the EF values were not increased correspondingly according to the SERS spectra and the EF values calculated above, respectively. It means that different morphology of Ag NP aggregation has different enhancement effects. From the high EF values for the mats with the PVA/Ag molar ratios of 530:1 and 530:3 corresponding to the dimer and short chain-like aggregation assembled in Ag/PVA nanofibers, respectively, we can conclude that, for Ag NPs, the dimer and a short chain-like structure are indeed the best optimized systems for achieving the highest possible enhancement. This result is to some extent similar to the report of the influence of particle number on the hot spots in strongly coupled Ag NP chains.[42]

Influence of Electrospinning Time. Figure 9a shows a set of SERS spectra of 4-MBA molecules absorbed on different electrospun mats with the same Ag/PVA solution (with PVA/Ag molar ratio of 530:2) but different electrospun time at an excitation wavelength of 514.5 nm. The corresponding EF values for SERS, as calculated with the equation mentioned above, are shown in Figure 9b. As the electrospinning time gradually increased from 10 to 30 min, the thickness of the mat increased and the amount of the Ag aggregates contained in nanofiber mats increased, thus the intensity of the Raman peaks increased observably and the EF values of the mats increased from 2.4×10^8 to 4.6×10^9 sharply. As the electrospinning time was further prolonged, the thickness of the mat and the gross amount of the Ag aggregates contained still increased, but the planar density of Ag aggregates on the per unit area of the Ag/PVA nanofiber mat and the number of 4-MBA molecules adsorbed on the per unit area of Ag/PVA nanofiber mats reached a saturated situation. Thus, the intensity of the Raman peak and the EF values only increased slightly and tended to be a constant finally.

When the two influence factors mentioned above were taken into account, the optimized Ag/PVA nanofiber mat was performed by electrospinning the Ag aggregate solution with PVA/Ag molar ratio of 530:1 or 530:3 for 1 h. It is noteworthy that the as-prepared Ag/PVA nanofiber mats own a high SERS activity for SERS measurements.

Comparison to Other Substrates for the Enhancement Ability. To evaluate the SERS performance of the Ag/PVA nanofiber mat, we prepared three different kinds of SERS substrates for comparison. The first one (substrate a) is a self-assembled Ag NP film formed by directly de-

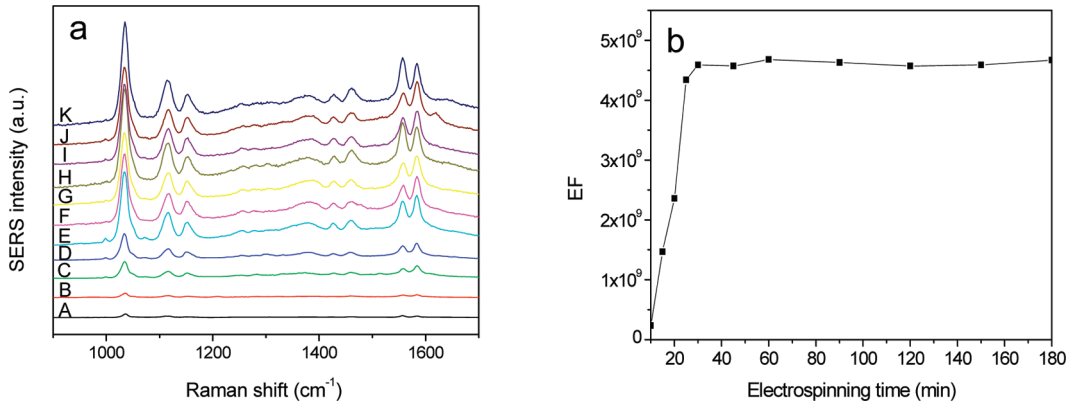

Figure 9. (a) SERS spectra of 2 mM 4-MBA molecules collected on a set of Ag/PVA nanofiber mats with different electrospinning time: (A) 10, (B) 15, (C) 20, (D) 25, (E) 30, (F) 45, (G) 60, (H) 90, (I) 120, (J) 150, and (K) 180 min. The molar ratio of PVA/Ag is 530:2, and the acquisition time is 5 s. (b) EF of 4-MBA molecules on a set of Ag/PVA nanofiber mats with different electrospinning time.

positing monodispersed starch-capped Ag NP aqueous solution on a clean quartz glass slide and dried in air at room temperature.[44] The second substrate (substrate b) is a nanofiber mat produced by electrospinning a sol−gel consisting of $AgNO_3$ and PVA, where Ag NPs scattered evenly throughout the surface of PVA nanofibers after reduced by UV lighting.[40,43] The third substrate (substrate c) is a casting film formed by dropping the as-prepared Ag/PVA blend solution on a clean quartz glass slide and dried in air at room temperature. The three substrates used for comparison (Figure 10) were fabricated by the solution with an equivalent concentration of Ag atoms as the solution fabricated for Ag/PVA nanofiber mats. The molar ratio of PVA/Ag in Ag/PVA nanofiber mats (substrate d) is 530:4, and the concentration of Ag atoms in the electrospinning solution is 10 mM. Although the concentration of Ag atoms in the solution used for preparation of substrates was equal, the planar density of each substrate was different on account of different surface area of the four substrates obtained.

The SERS spectra of 2 mM 4-MBA molecules obtained from the four substrates are shown in Figure 10d. The sample d showed the best SERS sensitivity in comparison to the other three substrates. To be specific, as we know, Ag aggregates have better SERS performance than the isolated Ag NPs, which has been demonstrated in our comparison that sample b was the weakest one. Second, the different aggregation states of Ag NPs showed different enhanced ability. The intensity of the Raman signals from sample a is more weak than that of samples c and d because sample a has less hot spots than samples c and d. For the two substrates with as-prepared Ag aggregates, the one assembled in PVA nanofibers with chain-like arrays (sample d) would be

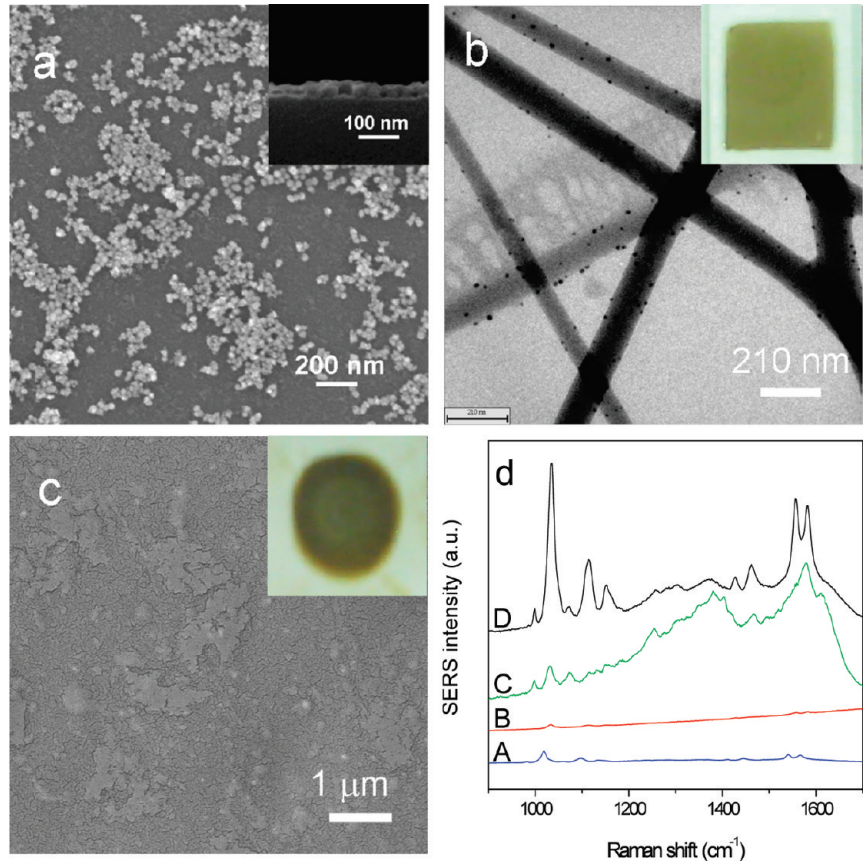

Figure 10. (a) Typical SEM images of the self-assembled Ag NP films. Inset image shows the cross section of the films. (b) Typical TEM image of nanofiber mats produced by electrospinning a sol−gel consisting of $AgNO_3$ and PVA and reduced by UV lighting. Inset image is the photograph of the nanofiber mats. (c) Typical SEM image of casting film formed by dropping the as-prepared Ag/PVA blend solution on a clean quartz glass slide and dried in air at room temperature. Inset image is the photograph of the casting film. (d) SERS spectra of 2 mM 4-MBA molecules collected on the corresponding substrates with 5 s acquisition time: (A) Substrate a. (B) Substrate b. (C) Substrate c. (D) Substrate d. The concentration of Ag atoms in the solution used for preparation of substrates was 10 mM.

more superior than the one dispersed in PVA membrane at random (sample c). So the morphologies of Ag aggregates with chain-like arrays made a significant contribution to the high sensitivity of SERS. Besides, the casting PVA film may have a high fluorescence background that would interfere with the Raman peaks.

Reproducibility and Stability of the SERS Substrate. The reproducibility of Raman signals from SERS spectra is of crucial importance for the use of SERS as a routine analytical tool. To test whether the as-prepared substrates are able to give reproducible SERS signals under a low concentration of target molecules, we collected SERS spectra of 4-MBA molecules with a concentration of 10^{-6} M from 15 randomly selected positions on the Ag/PVA nanofiber mat. The comparison results are shown in Figure 11.

The relative standard deviation (RSD) curve of 15 SERS spectra, which are used to estimate the reproducibility of SERS signals, is calculated by the method reported previously.[19] With this method, an overall impression and a detailed depiction of reproducibility can be provided. From the RSD-SERS graph (Figure 11), RSD values of signal intensities of all Raman peaks can be looked up directly, and to our substrates, the average RSD values of all Raman peaks are observed to be below 0.1, revealing a good reproducibility across the entire area of the Ag/PVA nanofiber mat even to a detection of a low concentration of target molecules. It should be noted that the RSD values corresponding to the major SERS peaks (Table 2) decreased in comparison with the average RSD value, which means the major SERS peaks have a good consistency and reproducibility, and once the interference of background has been excluded, the above-mentioned RSD values will drastically decrease. For our substrate, as far as the individual nanofibers are concerned, the Ag aggregates assembled in PVA nanofibers are not uniformed, but to the whole substrate, the Ag aggregates dispersed uniformly in PVA nanofibers, which would be demonstrated by a good reproducibility of SERS signals and the a RSD value curve from 15 randomly selected positions on the Ag/PVA nanofiber mats.

TABLE 2. RSD Values for the Major Peaks of the 4-MBA SERS Spectrum

peak position (cm^{-1})	1036	1117	1152	1557	1584
RSD value	0.071	0.069	0.062	0.071	0.078

For routine SERS analysis, the temporal stability of substrates is also important. To investigate this property, we compare the freshly prepared substrate and the substrate stored in air over 1 year for SERS detection of 4-MBA molecules. It is noted that neither a shift in the major Raman peaks nor a significant change in Raman intensity occurred, which is shown in Figure 12b. Furthermore, the substrate that has been used also possessed the temporal stability. We compared SERS measurements over 1 month after one treatment with 4-MBA solution to the freshly treated substrate. The SERS response of the substrate after use could be successfully measured only with a little decrease of the Raman intensity (Figure 12a). Such long lifetimes of our substrates are similar to the report about Ag NPs impregnated in polycarbonate substrate[20] for the same reason that there is almost no Ag NPs exposed to the atmosphere and the mechanical robustness and flexibility of the polymers while providing protection of Ag NPs from the surrounding environment to yield a high degree of temporal stability.

CONCLUSION

In summary, we have demonstrated a facile and new way to fabricate free-standing and flexible surface-enhanced Raman scattering (SERS) substrate, where high SM-SERS-active Ag dimer or aligned aggregates are assembled within poly(vinyl alcohol) (PVA) nano-

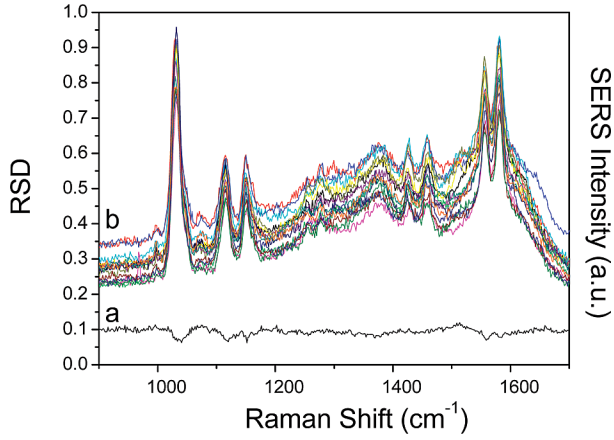

Figure 11. RSD-SERS graph. (a) RSD value curve of SERS of 10^{-6}M 4-MBA collected on the randomly selected 15 places on the Ag/PVA nanofiber mat. The molar ratio of PVA/Ag is 530:4, the electrospinning time is 1 h, and the acquisition time is 5 s. (b) Series of SERS spectra collected from the randomly selected 15 places on the Ag/PVA nanofiber mat.

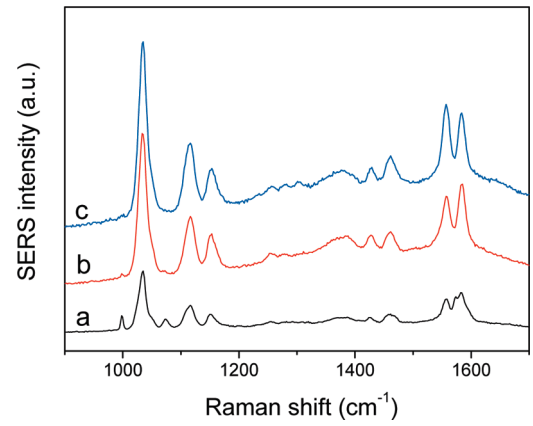

Figure 12. SERS spectra of 4-MBA molecules with concentration of 2 mM obtained from (a) the substrate have been used over 1 month, (b) the substrate stored in air over 1 year, and (c) the freshly prepared substrate. The substrate with PVA/Ag molar ratio is 530:4, and the electrospinning time is 1 h. The acquisition time is 5 s.

fibers with chain-like arrays by adjusting the quantity of Ag NPs dispersed in PVA solution in the electrospinning process. The results demonstrated that the degree of aggregation of Ag NPs in PVA nanofibers and the electrospinning time are two key factors determining the magnitude of SERS signal enhancement and the sensitivity of detection. The dimer and short chain-like structures of Ag NP aggregates have been demonstrated to be the best optimized system for achieving possibly the highest enhancement. The Ag NPs/PVA nanofiber mats have shown excellent detection reproducibility under a low concentration of 4-MBA molecule (10^{-6} M) detection with the average RSD values of the major Raman peak less than 0.07. This method represents a new strategy for the design of practical SERS substrates, which could offer a number of significant benefits over some conventional SERS substrates. The superiority of high sensitivity, reproducibility, stability, large-scale, cheap, and carry-home features are integrated in the obtained substrates. What is more, they are easy handled and disposable, which would bring a great convenience to the routine SERS detection and open an avenue for a wide range of application of SERS detection as a routine analytical tool.

METHODS

Materials. All reagents (analytical-grade purity) were purchased from Shanghai Chemical Reagents Co. and used without any further purification.

Synthesis Procedures of Silver Nanoparticles. Soluble starch (0.4 mmol) and L-lysine (0.16 mmol) were added to 4.0 mL of deionized water in a 10 mL microwave-sealed vessel. After that, a 4 mL aliquot of a 20 mmol aqueous solution of $AgNO_3$ was added and further stirred. The mixture heated to 150 °C by microwave under magnetic stirring and maintained at this temperature for 10 s. The obtained product was collected by centrifuging and washing with deionized water three times. The details of this process were discussed in our previous work.[44]

Preparation of Electrospinning Solution and Dimerization of Silver Nanoparticles. The as-prepared Ag NPs were redissolved in aqueous PVA (DP = 1750 ± 50, 99% hydrolyzed) solution (7 wt %, 5 mL) in a conical flask, followed by vigorous stirring in an incubator shaker at 40 °C for 5 h. Under the inducing effect of PVA, the aggregation occurred. Due to the high hydrophilic property, Ag NPs were miscible with hydrophilic polymers. So a viscous homogeneous gel of PVA and Ag NPs was obtained. The concentration of Ag atoms in the PVA solution was between 2.5 and 10 mM. The resulting green homogeneous solution was used for electrospinning and casting the Ag−PVA film.

Electrospinning and Casting Films. In a typical electrospinning process, the solution was electrospun at 20 kV positive voltage, 15 cm working distance (the distance between the needle tip and the grounded metal plate), and 0.3 mL/h flow rate at room temperature. The dense nonwoven mat of composite nanofibers was collected on the target.

For the preparation of casting films, 0.3 mL of the composite solution was dropped on a 2 cm × 2 cm clean quartz glass sheet and left to dry under ambient conditions to form the thin film.

Synthesis of SERS Samples. At first, the Ag/PVA nanofiber mat was immersed in a 5 mL 2 mM 4-mercaptobenzoic acid (4-MBA) ethanol solution for desired time (see Supporting Information Figure S8). Then, it was washed thoroughly with ethanol to remove unbound 4-MBA molecules and finally dried at room temperature to evaporate all of the ethanol.

Characterization. The phase purity of the as-prepared products was determined by X-ray diffraction (XRD) using a Philips X'Pert Pro Super X-ray diffractometer equipped with graphite monochromatized Cu Kα radiation (λ = 1.54178 Å). High-resolution transmission electron microscope (HRTEM) images were performed on a JEOL-2010 transmission electron microscope. Raman scattering spectra were recorded with a Renishaw System 2000 spectrometer using the 514.5 nm line of Ar^+ for excitation. UV−vis spectra were recorded on UV-2501PC/2550 at room temperature (Shimadzu Corporation, Japan). X-ray photoemission spectroscopy was recorded on ESCALAB-MK-II. IR spectrum was obtained by a Magna-IR-750 spectrometer. Microwave system was CEM Discover Microwave Synthesizer (CEM Corporation, USA).

Acknowledgment. S.-H.Y. acknowledges the funding support from the National Basic Research Program of China (2010CB934700), the Program of International S & T Cooperation (S2010GR0314), the National Natural Science Foundation of China (Nos. 50732006, 20671085), and the Partner-Group of the Chinese Academy of Sciences−The Max Planck Society.

Supporting Information Available: Histogram of the particle size distribution of Ag NPs, FTIR spectra of starch-capped Ag NPs and PVA-capped Ag aggregates, XPS of the electrospun Ag/PVA nonwoven mat, SEM image of the Ag/PVA nanofiber mat after immersed in 4-MBA ethanol solution, photograph of Ag/PVA nanofiber mat, which is easy to be tailored, Raman spectrum of aqueous 4-MBA solution (2 mM), and SERS spectra of 4-MBA molecules collected on Ag/PVA nanofibers mats with different concentrations and different incubation time are provided. This material is available free of charge *via* the Internet at http://pubs.acs.org.

REFERENCES AND NOTES

1. Fleischman, M.; Hendra, P. J.; McQuillan, A. J. Raman Spectra of Pyridine Adsorbed at a Silver Electrode. *Chem. Phys. Lett.* **1974**, *26*, 163–166.
2. Jeanmaire, D. L.; Van Duyne, R. P. Surface Raman Spectroelectrochemistry. Part I. Heterocyclic, Amromatic, and Aliphatic Amines Adsorbed on the Anodized Silver Electrode. *J. Electroanal. Chem.* **1977**, *84*, 1–20.
3. Albrecht, M. G.; Creighton, J. A. Anomalously Intense Raman Spectra of Pyridine at a Silver Electrode. *J. Am. Chem. Soc.* **1977**, *99*, 5215–5217.
4. Nie, S.; Emory, S. R. Probing Single Molecules and Single Nanoparticles by Surface-Enhanced Raman Scattering. *Science* **1997**, *275*, 1102–1106.
5. Doering, W. E.; Piotti, M. E.; Natan, M. J.; Freeman, R. G. SERS as a Foundation for Nanoscale, Optically Detected Biological Labels. *Adv. Mater.* **2007**, *19*, 3100–3108.
6. Qian, X.; Peng, X.-H.; Ansari, D. O.; Yin-Geon, Q.; Chen, G. Z.; Shin, D. M.; Yang, L.; Young, A. N.; Wang, M. D.; Nie, S. *In Vivo* Tumor Targeting and Spectroscopic Detection with Surface-Enhanced Raman Nanoparticle Tags. *Nat. Biotechnol.* **2008**, *26*, 83–90.
7. Jarvis, R. M.; Goodacre, R. Characterisation and Identification of Bacteria Using SERS. *Chem. Soc. Rev* **2008**, *37*, 931–936.
8. Mulvihill, M.; Tao, A.; Benjauthrit, K.; Arnold, J.; Yang, P. D. Surface-Enhanced Raman Spectroscopy for Trace Arsenic Detection in Contaminated Water. *Angew. Chem., Int. Ed.* **2008**, *47*, 6456–6460.
9. Gunawidjaja, R.; Peleshanko, S.; Ko, H.; Tsukruk, V. V. Bimetallic Nanocobs: Decorating Silver Nanowires with Gold Nanoparticles. *Adv. Mater.* **2008**, *20*, 1544–1549.
10. Aikensb, L. J. C. M.; Schatzc, G. C. Electronic Structure Methods for Studying Surface-Enhanced Raman Scattering. *Chem. Soc. Rev.* **2008**, *37*, 1061–1073.

11. Zhao, J.; Pinchuk, O. A.; Mcmahon, J. M.; Li, S. Z.; Ausman, L. K.; Atkinson, A. L.; Schatz, G. C. Methods for Describing the Electromagnetic Properties of Silver and Gold Nanoparticles. *Acc. Chem. Res.* **2008**, *41*, 1710–1720.
12. Banholzer, M. J.; Millstone, J. E.; Qin, L. D.; Mirkin, C. A. Rationally Designed Nanostructures for Surface-Enhanced Raman Spectroscopy. *Chem. Soc. Rev.* **2008**, *37*, 885–897.
13. Ko, H.; Singamaneni, S.; Tsukruk, V. V. Nanostructured Surfaces and Assemblies as SERS Media. *Small* **2008**, *4*, 1576–1599.
14. Abu Hatab, N. A.; Oran, J. M.; Sepaniak, M. J. Surface-Enhanced Raman Spectroscopy Substrates Created *via* Electron Beam Lithography and Nanotransfer Printing. *ACS Nano* **2008**, *2*, 377–385.
15. McFarland, A. D.; Young, M. A.; Dieringer, J. A.; Van Duyne, R. P. Wavelength-Scanned Surface-Enhanced Raman Excitation Spectroscopy. *J. Phys. Chem. B* **2005**, *109*, 11279–11285.
16. Brolo, A. G.; Arctander, E. R.; Gordon, B.; Leathem, K. L. Nanohole-Enhanced Raman Scattering. *Nano. Lett.* **2004**, *4*, 2015–2018.
17. Zhang, X. Y.; Zhao, J.; Whitney, A. V.; Elam, J. W.; Van Duyne, R. P. Ultrastable Substrates for Surface-Enhanced Raman Spectroscopy: Al_2O_3 Overlayers Fabricated by Atomic Layer Deposition Yield Improved Anthrax Biomarker Detection. *J. Am. Chem. Soc.* **2006**, *128*, 10304–10309.
18. Zhang, M. L.; Yi, C. Q.; Fan, X.; Peng, K. Q.; Wong, N. B.; Yang, M. S.; Zhang, R. Q.; Lee, S. T. A Surface-Enhanced Raman Spectroscopy Substrate for Highly Sensitive Label-Free Immunossay. *Appl. Phys. Lett.* **2008**, *92*, 043116-1–043116-3.
19. Zhang, B. H.; Wang, H. S.; Lu, L. H.; Ai, K. L.; Zhang, G.; Cheng, X. L. Large-Area Silver-Coated Silicon Nanowire Arrays for Molecular Sensing Using Surface-Enhanced Raman Spectroscopy. *Adv. Funct. Mater.* **2008**, *18*, 2348–2355.
20. Hasell, T.; Lagonigro, L.; Peacock, A. C.; Yoda, S.; Brown, P. D.; Sazio, P. J. A.; Howdle, S. M. Silver Nanoparticle Impregnated Polycarbonate Substrates for Surface Enhanced Raman Spectroscopy. *Adv. Funct. Mater.* **2008**, *18*, 1265–1271.
21. Ko, H.; Tsukruk, V. V. Nanoparticle-Decorated Nanocanals for Surface-Enhanced Raman Scattering. *Small* **2008**, *4*, 1980–1984.
22. Krug, J. T.; Wang, G. D.; Emory, S. R.; Nie, S. Efficient Raman Enhancement and Intermittent Light Emission Observed in Single Gold Nanocrystals. *J. Am. Chem. Soc.* **1999**, *121*, 9208–9214.
23. Emory, S. R.; Haskins, S.; Nie, S. Direct Observation of Size-Dependent Optical Enhancement in Single Metal Nanoparticles. *J. Am. Chem. Soc.* **1998**, *120*, 8009–8010.
24. Kneipp, K.; Wang, Y.; Kneipp, H.; Perelman, L. T.; Itzkan, I.; Dasari, R.; Feld, M. S. Single Molecule Detection Using Surface-Enhanced Raman Scattering (SERS). *Phys. Rev. Lett.* **1997**, *78*, 1667–1670.
25. Kneipp, K.; Kneipp, H.; Kneipp, J. Surface-Enhanced Raman Scattering in Local Optical Fields of Silver and Gold Nanoaggregates From Single-Molecule Raman Spectroscopy to Ultrasensitive Probing in Live Cells. *Acc. Chem. Res.* **2006**, *39*, 443–450.
26. Brus, L. Noble Metal Nanocrystals: Plasmon Electron Transfer Photochemistry and Single-Molecule Raman Spectroscopy. *Acc. Chem. Res.* **2008**, *41*, 1742–1749.
27. Marks, L. D.; Schatz, G. C.; Van Duyne, R. P. Probing the Structure of Single-Molecule Surface-Enhanced Raman Scattering Hot Spots. *J. Am. Chem. Soc.* **2008**, *130*, 12616–12617.
28. Kneipp, J.; Kneipp, H.; McLaughlin, M.; Brown, D.; Kneipp, K. *In Vivo* Molecular Probing of Cellular Compartments with Gold Nanoparticles and Nanoaggregates. *Nano Lett.* **2006**, *6*, 2225–2231.
29. Ko, H.; Chang, S.; Tsukruk, V. V. Porous Substrates for Label-Free Molecular Level Detection of Nonresonant Organic Molecules. *ACS Nano* **2009**, *3*, 181–188.
30. Culha, M.; Kahraman, M.; Tokman, N.; Türkğolu, G. Surface-Enhanced Raman Scattering on Aggregates of Silver Nanoparticles with Definite Size. *J. Phys. Chem. C* **2008**, *112*, 10338–10343.
31. Luo, L. B.; Yu, S. H.; Qian, H. S.; Zhou, T. Large-Scale Fabrication of Flexible Silver/Cross-Linked Poly(vinyl alcohol) Coaxial Nanocables by a Facile Solution Approach. *J. Am. Chem. Soc.* **2005**, *127*, 2822–2823.
32. Qian, H. S.; Luo, L. B.; Gong, J. Y.; Yu, S. H.; Li, T. W.; Fei, L. F. Te@Cross-Linked PVA Core−Shell Structures Synthesized by a One-Step Synergistic Soft-Hard Template Process. *Cryst. Growth Des.* **2006**, *6*, 607–611.
33. Zhan, Y. J.; Yu, S. H. Necklace-like Cu@Cross-Linked Poly(vinyl alcohol) Core−Shell Microcables by Hydrothermal Process. *J. Am. Chem. Soc.* **2008**, *130*, 5650–5651.
34. Polavarapu, L.; Xu, Q. H. Water-Soluble Conjugated Polymer-Induced Self-Assembly of Gold Nanoparticles and Its Application to SERS. *Langmuir* **2008**, *24*, 10608–10611.
35. Yang, Y.; Shi, J. L.; Tanaka, T.; Nogami, M. Self-Assembled Silver Nanochains for Surface-Enhanced Raman Scattering. *Langmuir* **2007**, *23*, 12042–12047.
36. Yang, Y.; Matsubara, S.; Nogami, M.; Shi, J. L.; Huang, W. M. One-Dimensional Self-Assembly of Gold Nanoparticles for Tunable Surface Plasmon Resonance Properties. *Nanotechnology* **2006**, *17*, 2821–2827.
37. Li, D.; Xia, Y. N. Electrospinning of Nanofibers: Reinventing the Wheel. *Adv. Mater.* **2004**, *16*, 1151–1170.
38. Greiner, A.; Wendorff, J. H. Electrospinning: A Fascinating Method for the Preparation of Ultrathin Fibers. *Angew. Chem., Int. Ed.* **2007**, *46*, 5670–5703.
39. Li, Z. Y.; Huang, H. M.; Wang, C. Electrostatic Forces Induce Poly(vinyl alcohol)-Protected Copper Nanoparticles to Form Copper/Poly(vinyl alcohol) Nanocables *via* Electrospinning. *Macromol. Rapid Commun.* **2006**, *27*, 152–155.
40. Saquing, C. D.; Manasco, J. L.; Khan, S. A. Electrospun Nanoparticle−Nanofiber Composites *via* a One-Step Synthesis. *Small* **2009**, *5*, 944–951.
41. Hunyadi, S. E.; Murphy, C. J. Bimetallic Silver−Gold Nanowires: Fabrication and Use in Surface-Enhanced Raman Scattering. *J. Mater. Chem.* **2006**, *16*, 3929–3935.
42. Wang, Z. B.; Luk'yanchuk, B. S.; Guo, W.; Edwardson, S. P.; Whitehead, D. J.; Li, L.; Liu, Z.; Watkins, K. G. The Influences of Particle Number on Hot Spots in Strongly Coupled Metal Nanoparticles Chain. *J. Chem. Phys.* **2008**, *128*, 094705-1–094705-5.
43. Barakat, N. A. M.; Woo, K. D.; Kanjwal, M. A.; Choi, K. E.; Khil, M. S.; Kim, H. Y. Surface Plasmon Resonances, Optical Properties, and Electrical Conductivity Thermal Hystersis of Silver Nanofibers Produced by the Electrospinning Technique. *Langmuir* **2008**, *24*, 11982–11987.
44. Hu, B.; Wang, S. B.; Wang, K.; Zhang, M.; Yu, S. H. Microwave-Assisted Rapid Facile "Green" Synthesis of Uniform Silver Nanoparticles: Self-Assembly into Multilayered Films and Their Optical Properties. *J. Phys. Chem. C* **2008**, *112*, 11169–11174.